NEUROSCIENCE
RESEARCH ARTICLE

INTERNATIONAL BRAIN IBRO RESEARCH ORGANIZATION

F. Brandalise et al. / Neuroscience xxx (2021) xxx–xxx

Dendritic Branch-constrained N-Methyl-D-Aspartate Receptor-mediated Spikes Drive Synaptic Plasticity in Hippocampal CA3 Pyramidal Cells

Federico Brandalise, [a,c*] **Stefano Carta,** [b] **Roberta Leone,** [a] **Fritjof Helmchen,** [b] **Anthony Holtmaat** [a*] **and Urs Gerber** [c†]

[a] *Department of Basic Neurosciences and the Center for Neuroscience, Centre Médical Universitaire (CMU), University of Geneva, 1211 Geneva, Switzerland*

[b] *Brain Research Institute and Neuroscience Center Zurich, University of Zurich, CH-8057 Zurich, Switzerland*

[c] *Former affiliation*[b]

Abstract—N-methyl-D-aspartate receptor-mediated (spikes can be causally linked to the induction of synaptic long-term potentiation (LTP) in hippocampal and cortical pyramidal cells. However, it is unclear if they regulate plasticity at a local or global scale in the dendritic tree. Here, we used dendritic patch-clamp recordings and calcium imaging to investigate the integrative properties of single dendrites of hippocampal CA3 cells. We show that local hyperpolarization of a single dendritic segment prevents NMDA spikes, their associated calcium transients, as well as LTP in a branch-specific manner. This result provides direct, causal evidence that the single dendritic branch can operate as a functional unit in regulating CA3 pyramidal cell plasticity.

Key words: dendrites, dendritic spike, plasticity, LTP, hippocampus, CA3.

INTRODUCTION

Each neuron in the brain receives thousands of synaptic inputs on its dendrites (London and Häusser, 2005; Hawkins and Ahmad, 2016), originating from local and recurrent neuronal circuits, as well as from long-range projecting neurons. Dendrites can integrate these inputs linearly (Cash and Yuste, 1998) such that when a sufficient number are active at the same time, the summed depolarization will reach the threshold for the generation of an action potential (AP) and hence lead to transfer of information to postsynaptic targets (Cash and Yuste, 1999). However, under certain conditions, co-active inputs can result in supralinear events called dendritic spikes (dSpikes) (Spruston, 2008; Major et al., 2013). dSpikes come in various forms and are usually classified based on their duration, threshold and most importantly the type of conductance that constitutes them. Generally, dSpikes fall into three main classes: sodium (Na^+) spikes (Ariav et al., 2003; Remy et al., 2009; Kim et al., 2015), calcium (Ca^{2+}) spikes (Kampa et al., 2006; Rancz and Häusser, 2006; Suzuki and Larkum, 2017), and N-methyl-D-aspartate receptor-mediated (NMDA) spikes (Major et al., 2008, Palmer et al., 2014, Augustinaite et al., 2014; for a comparison of the three types see also Antic et al., 2010, Stuart and Spruston, 2015). Due to the Ca^{2+} permeability of NMDA receptors, NMDA spikes are accompanied by a fast rise in the local dendritic cytosolic Ca^{2+} concentration (Chalifoux and Carter, 2011; Oikonomou et al., 2012; Kumar et al., 2018). In hippocampal pyramidal cells, such NMDAR-dependent, branch-specific Ca^{2+} transients have been described both *in vitro* (Makara and Magee, 2013; Brandalise et al., 2014, Basu et al., 2016) and *in vivo* (Sheffield and Dombeck, 2015; Sheffield et al., 2017; Rashid et al., 2020). They are positively correlated with AP discharges (Makara and Magee, 2013; Grienberger et al., 2014) as well as synaptic long-term potentiation (LTP) (Brandalise et al., 2016). However, despite the close relationship between local NMDA spikes and the induction of LTP in various brain areas (Gambino et al., 2014; Cichon and Gan, 2015; Bono and Clopath, 2017; Topolnik and Camiré, 2019), causal evidence is still lacking. The difficulty in establishing a causal link is in part due to the fact that NMDA spikes as measured at the soma may originate from multiple dendritic branches and hence affect plasticity processes globally. To determine the causal relationship between locally generated NMDA spikes and subsequent plasticity it is necessary to elicit and interrogate them locally at single dendritic branches.

Here, we use simultaneous electrical recordings from the soma and dendrite of CA3 pyramidal neurons, combined with Ca^{2+} imaging, to evaluate the role of

*Correspondence to: Federico Brandalise, Department of Basic Neurosciences and the Center for Neuroscience, Centre Médical Universitaire (CMU), University of Geneva, 1211 Geneva, Switzerland.
E-mail address: federico.brandalise@unige.ch (F. Brandalise).
† Currently retired.

https://doi.org/10.1016/j.neuroscience.2021.10.002
0306-4522/

locally generated NMDA spikes in synaptic plasticity. Local dendritic hyperpolarization prohibits the generation of branch-selective NMDA spikes and Ca^{2+} events, and prevents synaptic LTP. When NMDA spikes are generated in multiple branches, local hyperpolarization prevents Ca^{2+} events and LTP only in the recorded dendrite. Together, these data underscore a powerful causal relationship between locally triggered NMDA spikes and the induction of synaptic LTP.

EXPERIMENTAL PROCEDURES

Preparation of hippocampal slice cultures

All experiments described here were performed in rat organotypic slice cultures (Brandalise and Gerber, 2014; Brandalise et al., 2016), following a protocol approved by the Veterinary Department of the Canton of Zurich (approval ID 81–2014). The cultures were prepared from 6-day-old Wistar rats using the Gähwiler method (Gähwiler, 1981), which results in a quasi-monolayer of cells that facilitates dendritic imaging. Transverse slices were obtained (400 μm) and placed to coverslips with clotted chicken plasma. These were stored in sealed test tubes with serum-containing medium and maintained in a moving incubator at 36 °C for 21–28 days.

Patch-clamp recordings

Hippocampal slice cultures were mounted in an electrophysiological recording chamber under a 2-photon laser scanning microscope (2PLSM), which allows simultaneous electrophysiological recordings and calcium imaging. Slice cultures were maintained in an external recording solution (pH 7.4) containing (in mM): 137 NaCl, 2.7 KCl, 11.6 $NaHCO_3$, 0.4 NaH_2PO_4, 2 $CaCl_2$, 2 $MgCl_2$, 5.6 D-glucose and 0.001% phenol red to monitor pH. All experiments were performed at 34 °C. CA3 pyramidal cells were simultaneously recorded at the soma and a first-order dendritic branch using whole-cell recording patch pipettes. Somatic pipettes had a resistance between 5 and 7 MΩ and dendritic pipettes between 9 and 11 MΩ. Both somatic and dendritic patch pipettes were filled with internal solution (pH 7.2) containing (in mM): 135 K-gluconate, 5 KCl, 10 Hepes, 5 phosphocreatine, 2 MgATP, 0.4 NaGTP and 0.07 $CaCl_2$. For visualization of dendrites and calcium signals, cell filler Alexa Fluor 495 (Alexa-495; 10 μM) and the calcium dye Fluo-5F (100 μM) (both from Molecular Probes) were added to the internal solution. To prevent spontaneous APs or Na^+ dendritic spikes, QX-314 (500 nM) was included in the recording pipette. To reduce GABAa mediated responses, picrotoxin (1 mM) was included in the somatic electrode. Average resting membrane potential (RMP) of the recorded cells was −63.8 ± 4.6 mV (mean ± s.e.m.; n = 14). Voltage commands were corrected for the liquid junction potential (8.3 mV). Stimulation strength was calibrated to keep the postsynaptic responses below the AP threshold (amplitude 5.6 ± 1.1 mV for rCA3; 7.8 ± 1.6 mV for MF; measured at the soma; n = 14).

Stimulation paradigm

To activate rCA3 synaptic inputs in the apical dendritic tree, a theta-glass electrode was placed in the stratum radiatum of CA3, and to activate MF inputs, an electrode was placed in the dentate gyrus. The theta glass electrode (tip diameter = 5–20 μm) was filled with extracellular solution. Electrodes were located as close as possible (10–20 μm, see asterisks in Figs. 1A and 2A) to the apical dendrite in different locations until supralinear events were detected (upon pairing with MF inputs). The input timing dependent plasticity (ITDP) protocol consisted of 60 pairings at 0.1 Hz, with the MF inputs activated after the rCA3 inputs with a 10-ms delay. Stimulation intensities were set such that postsynaptic potentials remained below the action potential threshold. ITDP protocol 1 (ITDP1) included in addition to the rCA3-MF pairings a 25-ms long hyperpolarizing square current injection pulse starting at MF-stimulation onset (∼0.1 nA, resulting in ∼6 mV drop in membrane potential). ITDP protocol 2 (ITDP2) is identical to ITDP protocol 1 but without the hyperpolarizing square pulse. After accessing the cell with the somatic electrode, but before the ITDP protocol, part of the apical dendritic arbor was scanned to locate active branches by applying a few cycles of rCA3-MF stimulation pairings (∼5 on average; with an interval of 1 minute between stimulations in each FOV). Of the final two FOVs, one was centered on active branches, the other on inactive branches.

NMDA spike analysis

To identify the supralinear events (representing NMDA spikes) in the voltage recordings of each ITDP protocol, we first normalized all 60 traces to the amplitude of the baseline-evoked rCA3 EPSP. A histogram of the maximum amplitudes revealed a bimodal distribution. The traces representing the EPSP amplitudes that belonged to the first gaussian were considered linear responses, whereas those of the second gaussian were classified as NMDA spikes (for a more detailed explanation of the analysis see Brandalise et al., 2016). The NMDA spike probability was calculated as the ratio of the traces that were classified as NMDA spikes over the total number of traces (60). The normalized NMDA spike amplitude was represented as the percent increase from the amplitude of the mean linear response.

Two-photon Ca^{2+} imaging

For Ca^{2+} imaging, neurons were dialyzed with internal solution containing Fluo-5F (100 μM) and Alexa-495 through the dendritic recording pipette for at least 10 min before imaging was performed. Neurons were imaged using a 2PLSM (Scientifica) equipped with a Ti:sapphire laser (Tsunami, Spectra Physics) tuned to 840 nm and a 40x water-immersion objective lens (0.8 NA, Olympus). The laser power under the objective was typically between 10 and 15 mW. Emitted fluorescence was detected using two photomultiplier tubes, and spectrally separated using 525/50 nm (green channel)

Please cite this article in press as: Brandalise F et al. Dendritic Branch-constrained N-Methyl-D-Aspartate Receptor-mediated Spikes Drive Synaptic Plasticity in Hippocampal CA3 Pyramidal Cells. Neuroscience (2021), https://doi.org/10.1016/j.neuroscience.2021.10.002

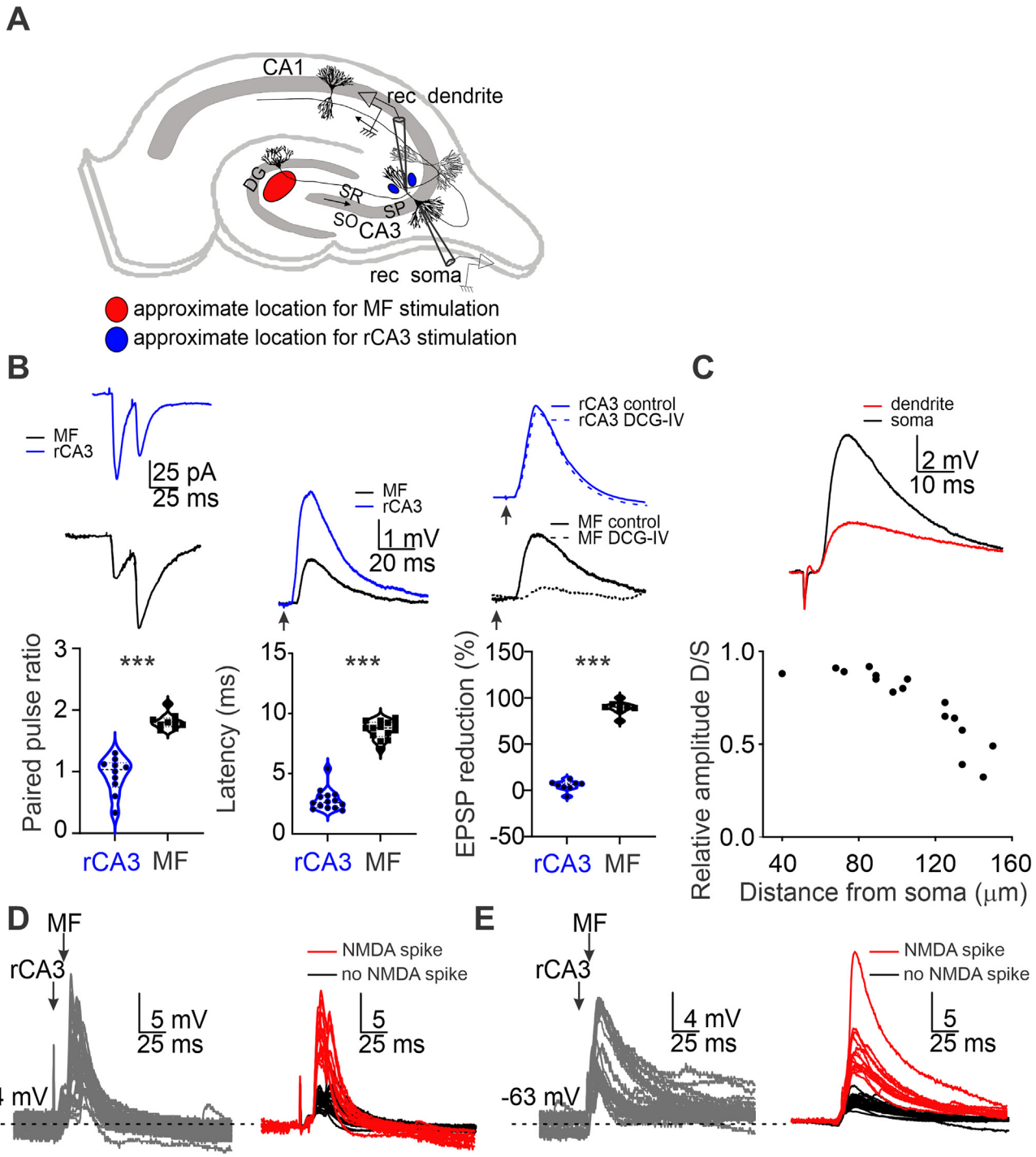

Fig. 1. Experimental configuration and differentiation between MF and rCA3 inputs. **(A)** Schematic depicting the positions of the recording and stimulation electrodes. The recording electrodes were placed in the stratum pyramidale (SP) and in the stratum radiatum (SR), respectively. Two stimulating electrodes were placed in the CA3 SR (blue) and in the dentate gyrus (DG; red) to excite CA3r and MF input, respectively. **(B)** Representative current traces of a paired stimulation with a 50-ms interval between the two pulses with the pooled data plots. Each point represents a recorded neuron. MF inputs to CA3 PCs evoke significant paired-pulse facilitation whereas rCA3 stimulation induce either paired-pulse facilitation or depression. The latency between the stimulation artefact and the EPSP is longer when stimulating MF as opposed to rCA3. Bath perfusion of DCG-IV (2 μM), an mGlu2R agonist, significantly reduces mossy fiber responses but not rCA3 responses. **(C)** The ratio of dendritic and somatically recorded EPSP amplitudes (D/S) upon MF stimulation, as a function of the distance of the dendritic recording pipette from soma. The negative relationship indicates that the ESPS are passively filtered along the dendrites. **(D, E)** Two dendritic recordings in which rCA3 and MF input stimulation with 10-ms delays (grey traces) frequently results in supralinear events (red traces) that can be distinguished from linear events (black traces) after normalization to the rCA3 EPSPs (see Methods). (For interpretation of the references to colour in this figure legend, the reader is referred to the web version of this article.)

Please cite this article in press as: Brandalise F et al. Dendritic Branch-constrained N-Methyl-D-Aspartate Receptor-mediated Spikes Drive Synaptic Plasticity in Hippocampal CA3 Pyramidal Cells. Neuroscience (2021), https://doi.org/10.1016/j.neuroscience.2021.10.002

and 620/60 nm (red channel) emission filters. Scanning and image acquisition were controlled by HelioScan software (Langer et al., 2013). Recordings of Fluo-5F fluorescence (Ca^{2+}) transients were acquired at a 10 Hz frame rate with the imaging fields (100 × 100 pixels, at a 0.3 μm/pixel resolution) encompassing several dendrites.

In order to record Ca^{2+} transients in several branches for each experiment, 2 FOVs were imaged alternatingly over the 60 pairings of the ITDP protocols, resulting in data sets consisting of 30 responses for each FOV. This was preferred over simultaneous data acquisition from multiple FOVs as this would have resulted in images with insufficient resolution for detailed analysis. We have previously found no change in the probability of evoking an NMDA spike over the time course of the 60 pairings (Supplementary Fig. 4 in Brandalise and Gerber, 2014).

At the end of each experiment, z-stacks of the fluorescently labelled cells were acquired to verify that the recorded neurons were indeed CA3 pyramidal cells. The z-stacks were also used to estimate the distance between the somatic and dendritic recording electrode. Data were analyzed with NIH ImageJ and Igor Pro (WaveMetrics) software. In ImageJ, dendritic segments were manually drawn as regions of interest (ROIs). Ca^{2+} signals were expressed as $\Delta F/F = (F - F_0)/F_0$ where F and baseline F_0 represent mean fluorescence values in an ROI. A Ca^{2+} transient was considered as a signal when its amplitude was greater than two times the standard deviation (s.d.) of the noise (~7%). Ca^{2+} transients that were temporally locked to the electrical stimulation were temporally integrated over a 2-s post-stimulus window, using custom-written scripts in MATLAB (units of '%s'; after subtraction of the mean $\Delta F/F$ in a 1-s pre-stimulus baseline window).

Statistical analysis

All data are expressed as the mean ± s.e.m. A total amount of 7 rats were used for this work. From each brain it was possible to obtain ~10–15 organotypic slices. 2 recordings per rat were included in the data set, and each recording was from a different slice culture. No data sets were excluded from analysis. Statistical analyses were performed using Origin 2016 (OriginLab) as well as GraphPad PRISM 2019. Statistical significance was calculated using non-parametric tests (Wilcoxon matched-pairs signed rank test for paired comparisons; Kruskal–Wallis test for comparison between more than two groups).

Data availability

The authors declare that the experimental results supporting the findings are included in the article and are available upon reasonable request.

RESULTS

Locally generated NMDA spikes are sufficient and necessary for rCA3 and MF pairing-induced LTP

Hippocampal CA3 pyramidal cells (PCs) receive excitatory input in a spatially segregated manner from mossy fibers (MFs) on the initial portions of apical and basal dendrites, from recurrent axons from neighboring CA3 pyramidal cells (rCA3s) on more medially located apical and basal dendrites, and from perforant-path axonal fibers originating in the entorhinal cortex on distal portions of the apical dendrites (Fig. 1A) (Amaral and Witter, 1989). Here, we performed dual electrical recordings from the soma and dendrites of single CA3 PCs in organotypic slice cultures of rat hippocampus, while sequentially stimulating rCA3 and MF afferents. By using theta-glass electrodes, we aimed at focal stimulation of rCA3 afferents close to CA3 PC dendrites (see Methods). This protocol has previously been shown to generate NMDA spikes and synaptic plasticity (Brandalise and Gerber, 2014; Brandalise et al., 2016). MF and rCA3 synapses onto CA3 PCs have been shown to be functionally distinct (Debanne et al., 1995; Kamiya et al., 1996; Salin et al., 1996; Mori et al., 2004). Therefore, to verify that we could independently stimulate these two inputs, we evaluated the properties of EPSPs generated by either the MF or rCA3 stimulation electrode. As compared to rCA3 inputs, MF inputs showed longer response onset latencies (8.4 ± 0.2 ms, $n = 8$ versus 2.8 ± 0.2 ms, $n = 8$; $P < 0.001$), paired pulse facilitation (1.81 ± 0.1 for MF, $n = 8$ versus 0.94 ± 0.1$n = 8$; $P < 0.001$) and much stronger sensitivity to DCG-IV, a selective mGluRII blocker (percentage of reduction 95.3 ± 2.3%, $n = 8$, $P < 0.001$ versus CA3r percentage of reduction 12 ± 1%, $n = 8$, $P = 0.19$; Fig. 1B). These distinct characteristics agree with previous findings (Brandalise and Gerber, 2014) and indicate that our electrode configuration provided selective access to either synaptic pathway. In addition, we found that MF-mediated depolarizations could passively spread to the medial portion of the dendrites as could be measured by the dendritic recording pipette (Fig. 1C), suggesting that MF inputs are able to interact with rCA3 inputs at the dendritic level. Indeed, the combined sequential stimulation of rCA3 and MF with a 10-ms delay induced supralinear events in a substantial fraction of the trials (red traces in Fig. 1D; see methods for classification criteria), which were previously shown to correspond to NMDA spikes (Brandalise and Gerber, 2014; Brandalise et al., 2016).

Before applying any plasticity protocols (Figs. 2 and 3) we first recorded baseline excitatory postsynaptic potentials (EPSPs) evoked by rCA3 stimulation alone for at least 10 mins (Fig. 2A, B). Since rCA3 axons make synaptic contacts mainly with secondary order dendrites, which branch off from the first order branches that we recorded from (Fig. 2A), the stimulation typically resulted in a greater amplitude and a faster rise time of

Please cite this article in press as: Brandalise F et al. Dendritic Branch-constrained N-Methyl-D-Aspartate Receptor-mediated Spikes Drive Synaptic Plasticity in Hippocampal CA3 Pyramidal Cells. Neuroscience (2021), https://doi.org/10.1016/j.neuroscience.2021.10.002

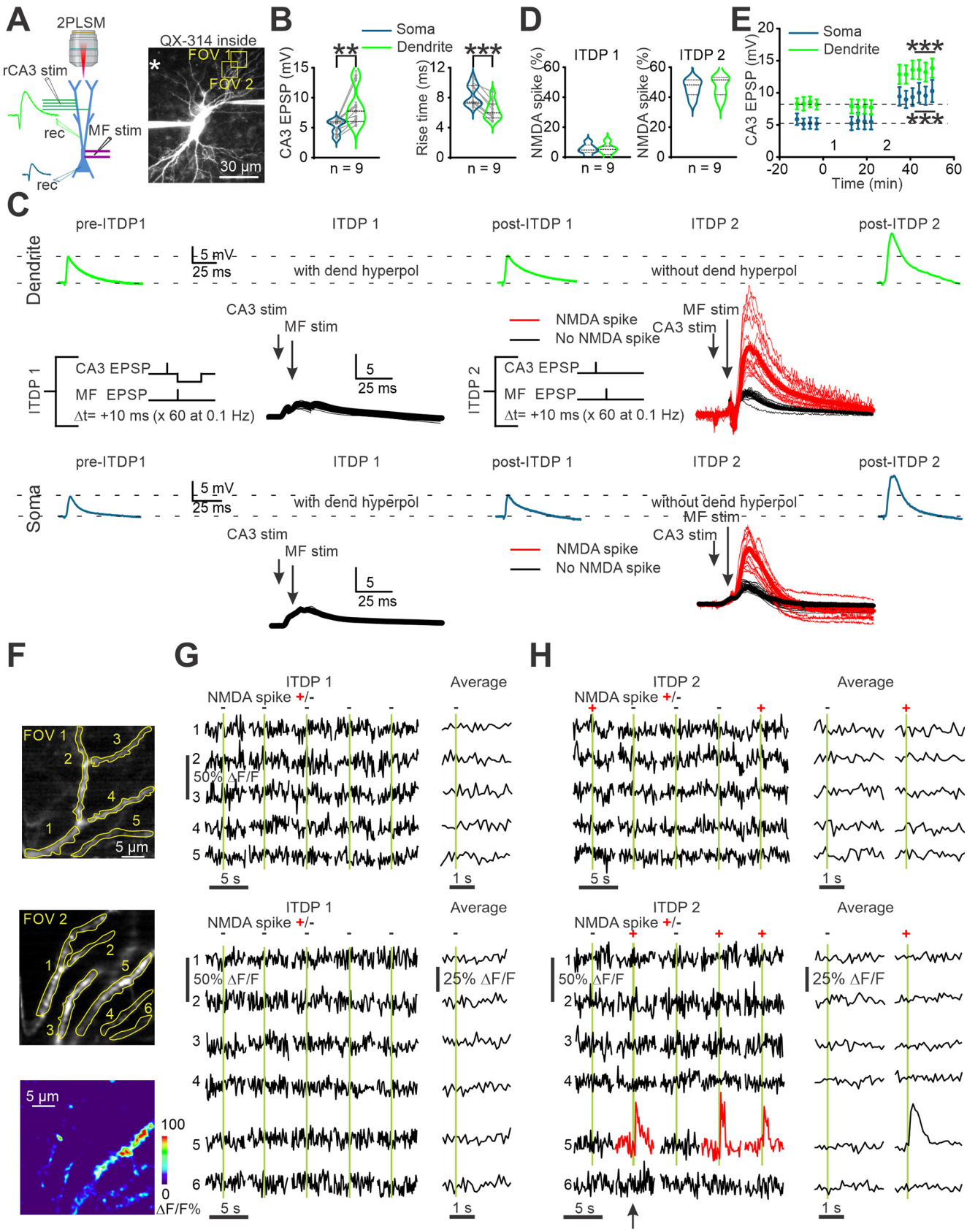

Please cite this article in press as: Brandalise F et al. Dendritic Branch-constrained N-Methyl-D-Aspartate Receptor-mediated Spikes Drive Synaptic Plasticity in Hippocampal CA3 Pyramidal Cells. Neuroscience (2021), https://doi.org/10.1016/j.neuroscience.2021.10.002

the postsynaptic response at the dendritic recording electrode (green) as compared to the somatic electrode (blue) (Fig. 2B; amplitude: 8.4 ± 3.1 mV for the dendrite; 5.0 ± 1.2 mV for the soma; $P = 0.005$; rise time: 6.4 ± 0.4 ms for the dendrite; 8.5 ± 0.5 ms for the soma; $P = 0.004$; $n = 9$). The dendritic rise times inversely correlated with the pipette's distance from the soma ($r = 0.63$; Fig. 4A). Similarly, the amplitude of the dendritically recorded rCA3 EPSPs correlated with the distance from the soma ($r = 0.80$; Fig. 4B). These data confirm that the electrotonic distance of the recording pipette to the rCA3 synaptic inputs decreases when the recordings are located closer to the apical dendritic tufts (Brandalise and Gerber, 2014).

Then we applied two input timing dependent plasticity (ITDP) protocols (Dudman et al., 2007) of 60 rCA3-MF paired stimuli at 0.1 Hz to evaluate the role of dendritic NMDA spikes in the induction of LTP at rCA3 synapses (Fig. 2C) (Brandalise et al., 2016). In the first protocol (ITDP1) we attempted to block NMDA spikes by applying hyperpolarizing current in the dendrite, whereas they were allowed to occur in the second (ITDP2). After each series of pairings, EPSPs evoked by only rCA3 stimulation were measured (post-ITDP EPSPs) and compared to the pre-ITDP EPSPs to assess the level of LTP. To rule out a possible contribution of spontaneous APs or dendritic Na^+ spikes during the protocol (Golding and Spruston, 1998), QX-314 (500 μM) was included in the dendritic recording pipettes.

We hypothesized that by hyperpolarizing the recorded dendrite we would reduce the opening of the voltage-dependent NMDA receptor channels mainly locally in this dendritic compartment and thereby prevent the triggering of NMDA spikes. Indeed, the negative current injection applied during ITDP1 (∼0.1nA for 25 ms, resulting in ∼6 mV drop in membrane potential), provided simultaneously with the MF simulation, almost entirely prevented the generation of NMDA spikes at both the dendritic compartment (fraction of pairing stimuli with non-linear events: 4.8 ± 1.6%, $n = 9$) and the soma (4.0 ± 1.4%, $n = 9$) (Fig. 2C, D). The amplitude of the rCA3 EPSPs was not affected by the ITDP1 protocol (soma: 5.2 ± 0.1 mV pre-ITDP1, 5.5 ± 0.1 mV post-ITDP1, $P = 0.4$, $n = 9$; dendrite: 7.7 ± 0.2 mV pre-ITDP1, 7.8 ± 0.1 mV post-ITDP1, $P = 0.7$, $n = 9$; Fig. 2D, E).

The ITDP2 pairing protocol, for which the same stimulation intensities were used as in ITDP1 but the hyperpolarization step was omitted, successfully evoked NMDA spikes in a considerable fraction of the rCA3-MF pairings, significantly higher compared to ITDP1 and visible at both the dendrite (49.5% ± 3.5%, $P = 0.001$ vs ITDP1, $n = 9$), and the soma, albeit with a dampened amplitude (48.6 ± 3.4%, $P = 0.002$ vs ITDP1, $n = 9$) (Fig. 2C, D). The fraction of trials that produced NMDA spikes (recorded at the dendrite) increased with the distance of the recording pipette to the soma ($r = 0.53$; Fig. 4C), suggesting that they are generated locally in the more medial portions of the dendritic tree where the rCA3 synapses are located. In contrast to ITDP1, ITDP2 caused significant increase in the rCA3 EPSP amplitude at the dendritic compartment (7.8 ± 0.1 mV pre-ITDP2; 13.4 ± 0.4 mV post-ITDP2, $P = 0.0004$, $n = 9$) as well as at the soma (5.5 ± 0.1 mV pre-ITDP2; 9.6 ± 0.5 mV post-ITDP2, $P = 0.0001$, $n = 9$) for the whole duration of the recordings after ITDP2 (up to 20 min). This data confirms our previous observation that the repeated sequential pairing of MF and rCA3 inputs selectively drives LTP of the rCA3 inputs (and not of MF inputs; Brandalise and Gerber, 2014; Brandalise et al., 2016).

We asked whether the effect of the different stimulation protocols might also visible in the dendritic Ca^{2+} signals, which we previously showed are associated with the NMDA spikes (Brandalise et al., 2016). Simultaneous 2PLSM imaging of Fluo-5F in at least 2 different fields of view (FOVs) (∼30 stimulations each; Fig. 2F; Methods) revealed a negligible fraction of local Ca^{2+} transients in coincidence with the paired stimulations during ITDP1 (2.2 ± 0.4%, $n = 9$; Fig. 1G, H), whereas such events were readily detected in the same FOVs during ITPD2 (45.6 ± 4.3%, $n = 9$; Fig. 2G, H). The Ca^{2+} transients remained confined to single branches (width: 13.5 ± 2.2 μm, $n = 9$ cells), and were detected in at least one of the branches connected to the recording electrode ($\Delta F/F = 63 \pm 6$ %, $n = 9$;

Fig. 2. Local dendritic hyperpolarization prevents focal stimulation-evoked NMDA spikes and LTP. **(A)** Left, schematic of the dendritic and somatic patch-clamp recordings in CA3 cells, and the paired stimulation of rCA3 and MF inputs. rCA3 axons are focally stimulated near the dendritic electrode, which predominately activates synapses on the recorded dendrite. Right, a CA3 pyramidal neuron filled with Fluo-5F and Alexa-495, imaged in the Alexa channel, which visualizes the soma, dendrites as well as the somatic and dendritic electrodes. FOV 1 and 2 refer to the examples provided in **(F–H)**. **(B)** Focal stimulation of rCA3 inputs results in larger amplitudes and shorter rise times of the EPSPs in the dendritic (green) as compared to the somatic (blue) recordings ($P = 0.005$; $P = 0.004$) **(C)** Protocols for input timing dependent plasticity (ITDP), consisting of rCA3-EPSPs baseline recordings (pre-ITDP) followed by 60 paired rCA3 and MF stimulations at 0.1 Hz, and another series of rCA3-EPSP recordings (post-ITDP), both at the dendrite (green) and the soma (blue). During the first series of pairings (ITDP 1) a hyperpolarizing step was delivered through the dendritic recording pipette immediately following mossy fiber stimulation. In the second series of pairings (ITDP 2) this hyperpolarization step was omitted. During ITDP 1, only linear responses (black traces) could be detected at the soma and dendrite, and the post-ITDP 1 rCA3 EPSP amplitude was similar to the pre-ITDP 1 EPSP. During ITDP2, NMDA spikes (red traces) were also detected both at the soma and the dendrite, and the post-ITDP2 rCA3 EPSP amplitude was increased. **(D)** Pooled data for the percentage of paired stimulations that evoked NMDA spikes during ITDP 1 and ITDP 2 at the soma (blue) or at the dendrites (green). **(E)** Pooled data for the rCA3 EPSP amplitudes normalized to baseline after ITDP 1 (1) and ITDP 2 (2), indicating a significant increase after ITDP 2 ($P = 0.0004$). **(F)** Top, examples of pairing-evoked Ca^{2+} transients in two portions of the dendritic tree (FOV 1 and FOV 2) of the recorded cell. The lines delimit the individual dendritic branches in which the transients were analyzed. Bottom, the Fluo-5F $\Delta F/F$ fluorescence change for one pairing trial (arrow in **(H)**). **(G)** Example Ca^{2+} transients from the ROIs in **(F)**, recorded during 5 representative consecutive pairings (green bars) during ITDP 1. Trials with linear ("−") and supralinear ("+") EPSP summation are indicated. Ca^{2+} transients for FOV1 and FOV2 were averaged separately for linear and supralinear trials. **(H)** Same as **(H)** but during ITDP 2. (For interpretation of the references to colour in this figure legend, the reader is referred to the web version of this article.)

Please cite this article in press as: Brandalise F et al. Dendritic Branch-constrained N-Methyl-D-Aspartate Receptor-mediated Spikes Drive Synaptic Plasticity in Hippocampal CA3 Pyramidal Cells. Neuroscience (2021), https://doi.org/10.1016/j.neuroscience.2021.10.002

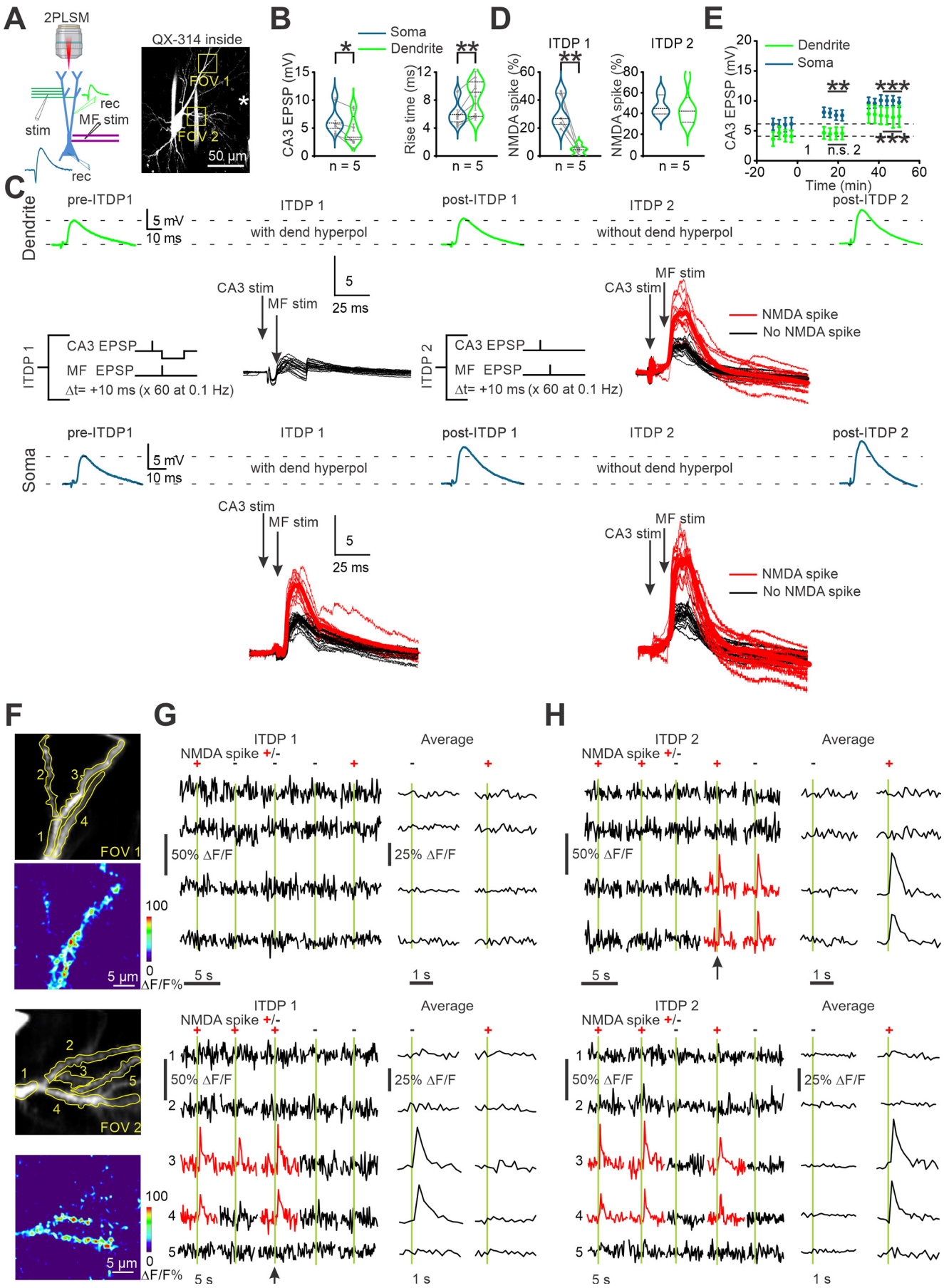
A
2PLSM
QX-314 inside
FOV 1
FOV 2
50 µm
rec
MF stim
stim
rec
B
Soma
Dendrite
CA3 EPSP (mV)
Rise time (ms)
n = 5
n = 5
D
ITDP 1
ITDP 2
NMDA spike (%)
NMDA spike (%)
n = 5
n = 5
E
Dendrite
Soma
CA3 EPSP (mV)
n.s.
Time (min)
C
Dendrite
pre-ITDP1
5 mV
10 ms
ITDP 1
with dend hyperpol
post-ITDP 1
ITDP 2
without dend hyperpol
post-ITDP 2
CA3 stim
MF stim
5
25 ms
ITDP 1
CA3 EPSP
MF EPSP
Δt= +10 ms (x 60 at 0.1 Hz)
ITDP 2
CA3 EPSP
MF EPSP
Δt= +10 ms (x 60 at 0.1 Hz)
NMDA spike
No NMDA spike
Soma
pre-ITDP1
5 mV
10 ms
ITDP 1
with dend hyperpol
post-ITDP 1
ITDP 2
without dend hyperpol
post-ITDP 2
CA3 stim
MF stim
5
25 ms
NMDA spike
No NMDA spike
F
FOV 1
5 µm
100
0
ΔF/F%
FOV 2
5 µm
100
0
ΔF/F%
G
ITDP 1
NMDA spike +/-
Average
50% ΔF/F
25% ΔF/F
5 s
1 s
ITDP 1
NMDA spike +/-
Average
50% ΔF/F
25% ΔF/F
5 s
1 s
H
ITDP 2
NMDA spike +/-
Average
50% ΔF/F
5 s
1 s
ITDP 2
NMDA spike +/-
Average
50% ΔF/F
25% ΔF/F
5 s
1 s

Fig. 1I) in high coincidence with the supralinear potentials (92.2 ± 4.5%, n = 9). In accordance with the electric dendritic recordings, the amplitude of the Ca^{2+} transients increased with the distance from the soma (r = 0.61, Fig. 4D), which supports the notion that NMDA spikes are generated locally and close to the rCA3 synapses. Together, this data shows that the reduction of NMDA channel openings at a segment of the dendritic tree prevents the local onset of NMDA spikes and consequently the induction of LTP.

NMDA spikes are independently generated at different branches and induce branch-constrained LTP

In a second set of experiments we placed the theta glass electrode slightly more distal from the dendritic electrode. We reasoned that this may lead to a strong activation of more dendritic branches than the one we were recording from (see schematic in Fig. 3A). Indeed, stimulation resulted in postsynaptic responses with lower amplitudes and slower rise times at the dendritic compartment (green) as compared to the soma (blue) (Fig. 3B; amplitude: 3.9 ± 1.0 mV dendrite, 6.2 ± 1.0 m V soma, P = 0.01; rise time: 7.8 ± 1.0 ms dendrite, 5. 7 ± 0.7 ms soma; P = 0.007; n = 5). This confirms that the majority of the activated synapses were on average in closer proximity to the somatic recording electrode than to the recorded dendritic compartment.

Similar to the first set of experiments, we delivered two ITDP pairing protocols, the first one while hyperpolarizing the recorded dendrite with a negative current injection (ITDP1, Fig. 3C), and a second while leaving the resting membrane potential unaltered (ITDP2, Fig. 3C). Again, we reasoned that a local hyperpolarization should mainly affect the recorded dendrite and to a lesser extent the rest of the dendritic tree. Hence, because the majority of the activated rCA3 inputs are presumably broadly distributed over the dendritic tree, their capacity to trigger NMDA spikes at other locations should not, or only slightly, be affected. Consistent with this hypothesis, during ITDP1, no NMDA spikes were detected in the recorded dendritic compartment (3.7 ± 1.3%, n = 5), whereas a significantly higher number could be identified through the somatic electrode (30.8 ± 4.6%, n = 5, P = 0.003). The latter events putatively originated from branches in parts of the dendritic tree different from where the recorded compartment was located. The absence of NMDA spikes at the hyperpolarized dendritic compartment was not due to a lack of converging inputs on this segment, since numerous supralinear events could be detected upon the omission of the hyperpolarizing step during ITDP2 (Fig. 3C). In fact, ITDP2 evoked a similar number of supralinear events at both the dendritic and somatic compartments (57.4 ± 4.2% for the soma; 56.1 ± 3.7% for the dendrite, n = 5, P = 0.2). Nonetheless, at the soma they had a higher amplitude as compared to those triggered during ITDP1 (from 7.3 ± 0.7 mV to 10.4 ± 1.1 mV, P = 0.002, n = 5, Fig. 3C), presumably due to the summation of the depolarization induced by the NMDA spikes originated at the two different dendritic compartments (FOV1 and FOV2) and converging at the soma.

Upon both ITDP1 and ITDP2, we found a significant increase in the rCA3 EPSPs at the soma (Fig. 3C; ITDP1: from 5.9 ± 0.2 mV to 7.8 ± 0.3 mV, P = 0.005, n = 5; ITDP2: from 7.8 ± 0.3 mV to 10.2 ± 0.9 mV, P = 0.0007, n = 5), indicating that LTP had been induced at a broad number of synapses. Interestingly, only a small increase in rCA3 EPSP amplitudes was detected at the dendritic compartment upon ITDP1, but this was statistically non-significant (from 4.1 ± 0.4 mV pre-ITDP1 to 4.5 ± 0.1 mV post-ITDP1, P = 0.08, n = 5). This increase became statistically significant after release of the local hyperpolarization step during

Fig. 3. Local dendritic hyperpolarization does not prevent stimulus-evoked NMDA spikes and LTP in branches other than the recorded dendrite. **(A)** Left, schematic of the dendritic and somatic patch-clamp recordings in CA3 cells, and the paired stimulation of rCA3 and MF inputs. rCA3 axons distant from the recording electrode are stimulated, which predominantly activates synapses that are not located on the recorded dendrite. Right, a CA3 pyramidal neuron filled with Fluo-5F and Alexa-495, imaged in the Alexa channel, which visualizes the soma, dendrites as well as the somatic and dendritic electrodes. FOV 1 and 2 refer to the examples provided in **(F–H)**. **(B)** distant stimulation of rCA3 inputs results in smaller amplitudes and longer rise times of the EPSPs in the dendritic (green) as compared to the somatic (blue) recordings (P = 0.01, P = 0.007). **(C)** Protocols for input timing dependent plasticity (ITDP), consisting of rCA3-EPSPs baseline recordings (pre-ITDP) followed by 60 paired rCA3 and MF stimulations at 0.1 Hz, and another series of rCA3-EPSP recordings (post-ITDP), both at the dendrite (green) and the soma (blue). During the first series of pairings (ITDP 1) a hyperpolarizing step was delivered through the dendritic recording pipette immediately following mossy fiber stimulation. In the second series of pairings (ITDP 2) this hyperpolarization step was omitted. During both ITDP 1 and ITDP 2, linear responses (black traces) and NMDA spikes (red traces) could be detected at the soma and dendrite. For both protocols, the post-ITDP rCA3 EPSPs amplitudes were increased at the soma, but only for ITDP 2 at the dendrite. **(D)** Pooled data for the percentage of paired stimulations that evoked NMDA spikes during ITDP 1 and ITDP 2 at the soma (blue) or at the dendrites (green) **(E)** Pooled data for the rCA3 EPSP amplitudes normalized to baseline after ITDP 1 (1) and ITDP 2 (2), indicating a significant increase after ITDP 1 and 2 **(F)** Top images, examples of pairing-evoked Ca^{2+} transients in two portions of the dendritic tree (FOV 1 and FOV 2) of the recorded cell. The lines delimit the individual dendritic branches in which the transients were analyzed. Bottom images, the Fluo-5F $\Delta F/F$ fluorescence change for one pairing trial (arrows in **(G, H)**). **(G)** Example Ca^{2+} transients from the ROIs in **(F)**, recorded during 5 representative consecutive pairings (green bars) during ITDP 1. Trials with linear ("−") and supralinear ("+") EPSP summation are indicated. Ca^{2+} transients for FOV1 and FOV2 were averaged separately for linear and supralinear trials. **(H)** Same as **(H)** but during ITDP 2. **(D)** Pooled data for the percentage of NMDA spikes during ITDP 1 and ITDP 2 both in the soma (blue) and in the dendrites (green). **(E)** Plots of EPSP time course. **(F)** Same CA3 pyramidal neuron labelled with Fluo-5F **(F)** Fluorescence measurements to detect pairing-induced Ca^{2+} transients were obtained in 4 ROIs in FOV 1 and 5 ROIs in FOV 2 for different portion of apical dendritic branches. Middle and bottom image shows localized Fluo-5F $\Delta F/F$ fluorescence change for one pairing trial (indicated by a black arrow in **(H)** or **(I)**). **(H)** Example Ca^{2+} transients from ROIs selected in **(G)**, recorded during 5 representative consecutive pairings in ITDP 1 (green bars). Trials with linear ("−") and supralinear ("+") EPSP summation are indicated. Ca^{2+} transients for FOV1 and FOV2 were averaged separately for linear and supralinear trials. (For interpretation of the references to colour in this figure legend, the reader is referred to the web version of this article.)

Please cite this article in press as: Brandalise F et al. Dendritic Branch-constrained N-Methyl-D-Aspartate Receptor-mediated Spikes Drive Synaptic Plasticity in Hippocampal CA3 Pyramidal Cells. Neuroscience (2021), https://doi.org/10.1016/j.neuroscience.2021.10.002

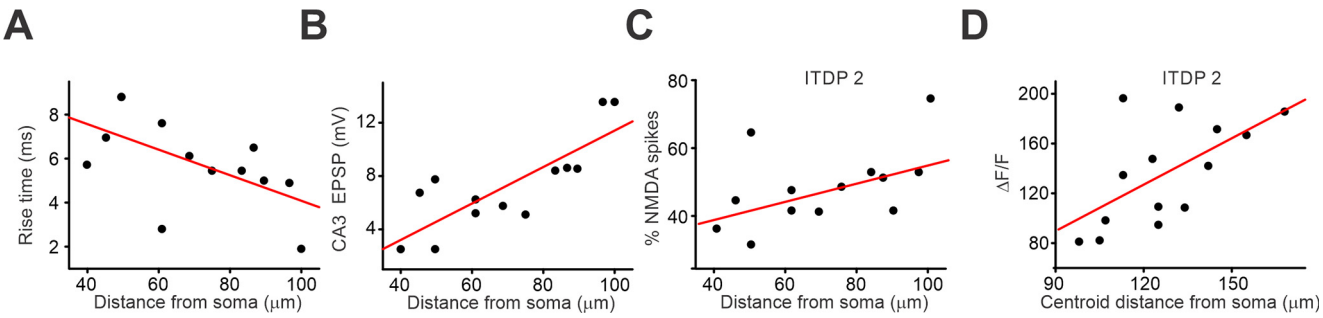

Fig. 4. Correlation of rCA3-evoked EPSPs and MF-rCA3-evoked NMDA spikes with the distance along the dendritic tree. Rise time **(A)** and amplitude **(B)** of rCA3 EPSPs as a function of the distance of the dendritic electrode location from the soma. Percentage of NMDA spikes **(C)** and amplitude of the branch-constrained calcium transients detected during the ITDP 2 protocol **(D)** as a function of the distance of the dendritic electrode location from the soma.

ITPD2 (from 5.5 ± 0.1 mV pre-ITDP2 to 8.3 ± 0.5 mV post-ITDP2, $P = 0.0003$, $n = 5$). Together, this suggests that NMDA spikes generated at various places in the dendritic tree do not readily induce LTP in branches that remain hyperpolarized during the pairing, which is consistent with the NMDAR-dependency of synaptic LTP.

The results of the electrophysiological analysis were confirmed by the Ca^{2+} imaging data. Using simultaneous 2PLSM from 2 FOVS (Fig. 3F), we failed to detect dendritic Ca^{2+} transients in the recorded dendritic compartment (Fig. 3G, H, 3.7 ± 1.2% for FOV1, $n = 5$) but we did detect events on other branches (57.8 ± 9.6%, for FOV2). The Ca^{2+} transients in FOV2 had a very high coincidence with the NMDA spikes recorded at the soma (89.4 ± 3.4% $n = 5$). Interestingly, the amplitudes of the Ca^{2+} transients in FOV2 were not significantly different between ITDP1 and ITDP2 (ITDP1: $\Delta F/F = 57.2 \pm 12.3\%$; ITDP2: $\Delta F/F = 59.8 \pm 14.2\%$, $P = 0.8$, $n = 5$) as well as the spatial spread of the Ca^{2+} signal within the branch (11.7 ± 2.4 μm, $P = 0.7$, $n = 5$). This demonstrates that the Ca^{2+} influx detected at each branch was not propagating or diffusing to the neighboring dendrites. Instead they remained confined to the region where they originated, independently of the numbers of the activated branches.

DISCUSSION

We investigated the role of localized NMDA spikes in inducing LTP at recurrent synapses of CA3 cells in rat hippocampal slices, using dendritic and somatic patch clamp recordings combined with simultaneous imaging of dendritic Ca^{2+} transients. We induced NMDA spikes and LTP using an ITDP protocol that consisted of the repetitive paired stimulation of rCA3 and MF inputs (Brandalise and Gerber, 2014). In this protocol the activation of MF inputs on the apical trunk (with a 10-ms delay after the rCA3 activation) generates a powerful subthreshold response that relieves the magnesium block at rCA3 synapses, and thereby acts as a gate for the induction of supralinear NMDA-mediated synaptic responses and LTP at rCA3 synapses (Brandalise and Gerber, 2014). By using focal synaptic stimulation of rCA3 fibers we met the biophysical requirements for inducing NMDA spikes (Schiller et al., 2000), i.e. the activation of a cluster of synapses on a few targeted branches along with the opening of extra-synaptic receptors (Larkum and Nevian, 2008; Chalifoux and Carter, 2011; Kleindienst et al., 2011; Oikonomou et al., 2012). Despite the fact that we could only target primary dendrites with our recording electrodes, the simultaneous use of 2PLSM revealed that the rise of cytosolic Ca^{2+}, which is associated with the NMDA spikes, originated preferentially in the thinner, secondary-order dendrites, as previously described (Polsky et al., 2004; Losonczy et al., 2008; Branco et al., 2010). By using a local hyperpolarization step, applied via the dendritic electrode, we prevented the focal stimulation from triggering NMDA spikes along the patch-clamped dendrite, which confirms that the initiation of these spikes depends on local, presumably synaptic mechanisms (Lisman, 2017). The local hyperpolarization also countered an increase of rCA3 non-paired synaptic responses, which would normally occur after multiple pairings (Brandalise et al., 2016). This indicates that subthreshold responses *per se* do not induce LTP, which confirms the strong dependency of synaptic plasticity on dSpikes in this paradigm (Brandalise et al., 2016). The absence of a potentiation effect was not due to a lack of synaptic mechanisms for LTP at other locations, since a second ITDP protocol in which hyperpolarization was omitted did evoke LTP. These results did not, however, exclude the possibility that the dendritic hyperpolarization had prevented opening of NMDA receptors on other branches. By moving the stimulation electrode further away from the dendritic recording electrode, we were able to activate synapses located on other branches. This allowed us to test how a local hyperpolarization of one dendritic segment would impact synapses on adjacent branches. In this experiment, the local hyperpolarization did not prevent the generation of NMDA spikes in other branches, as shown by 2PLSM of Ca^{2+} events, as well as by the occurrence of supralinear events at the soma. Interestingly, under these conditions LTP could be evoked as measured at the soma, which was likely due to plasticity of synapses at distant locations from the recorded dendrite. Indeed, and not unexpectedly, LTP was not observed at the dendritic compartment that was hyperpolarized. This is in line

Please cite this article in press as: Brandalise F et al. Dendritic Branch-constrained N-Methyl-D-Aspartate Receptor-mediated Spikes Drive Synaptic Plasticity in Hippocampal CA3 Pyramidal Cells. Neuroscience (2021), https://doi.org/10.1016/j.neuroscience.2021.10.002

with the finding that this type of LTP depends on synaptic NMDA receptors (Dudman et al., 2007; Losonczy et al., 2008; Brandalise and Gerber, 2014; Brandalise et al., 2016).

Taken together, our data support the hypothesis that NMDA spikes and their associated Ca^{2+} transients can be generated locally in single dendritic branches of CA3 cells (Branco and Häusser, 2010) and that these branch-constrained NMDA spikes can trigger LTP separately from one another, and thus act as unitary modules for synaptic plasticity (Branco and Häusser, 2011; Kastellakis et al., 2015; Mel et al., 2017; Kastellakis and Poirazi, 2019; Poirazi and Papoutsi, 2020).

What is the physiological relevance of this type of plasticity (Golding et al., 2002; Lisman and Spruston, 2005; Remy and Spruston, 2007)? As argued previously, the giant synapses of the MF inputs are thought to have a detonator-like effect on CA3 neurons, which would be necessary for spike-timing-dependent LTP (Lisman and Spruston, 2010). However, MF inputs, originating from sparsely firing dentate granule cells do not readily evoke long bursts of action potentials *in vivo*, and thus it has been debated as to whether synapses of the local circuitry could undergo efficient plasticity (Henze et al., 2002). In accordance with previous work, we show here that the strong subthreshold depolarization as induced by MF inputs allows the generation of local NMDA spikes in more distal dendrites, which is as powerful or perhaps even more efficient in inducing LTP than back-propagating APs (Hardie and Spruston, 2009). Therefore, in behaving animals, appropriately timed subthreshold MF input could trigger LTP of theta-timed inputs onto CA3 cells from neighboring CA3 cells, and provide a framework for hippocampal neuronal ensemble formation that is implicated in memory. Could the local prevention of dSpike generation be physiologically relevant? Despite the fact that the square hyperpolarization step that we applied is highly artificial, it could mimic the effects of physiological events. For example, local dendritic inhibition can evoke compartment-specific hyperpolarization (Murayama et al., 2009; Dorsett et al., 2021). Such forms of inhibition may gate the induction of plasticity in protocols where dSpikes have been observed to be effectors (Cichon and Gan, 2015; Doron et al., 2017; Williams and Holtmaat, 2019). Other studies have described an inhibitory effect of somatostatin-expressing interneurons on the coupling between NMDA spikes and somatic bursting (Lovett-Barron et al., 2012). Activation of interneurons can also negatively affect the calcium influx occurring during a back-propagating action potential (Müllner et al., 2015). It is feasible that a similar mechanism is involved in modulating branch-constrained calcium transients associated with local NMDA spikes. For instance, interneurons interneurons targeting the upper cortical layer (such as Martinotti cells) can control dendritic spikes on the apical part of the layer 5 pyramidal cells; basket cells on the contrary are more prone to modulate the calcium spikes occurring in the main trunk of the same pyramidal cell (Gidon and Segev, 2012). The local hyperpolarization could also mimic the activity-dependent modulation of particular ion channel conductances at dendritic nodes, which have been shown to strongly regulate local dSpike generation (Soldado-Magraner et al., 2020; Humphries et al., 2021).

DECLARATION OF COMPETING INTEREST

The authors declare that they have no known competing financial interests or personal relationships that could have appeared to influence the work reported in this paper.

ACKNOWLEDGEMENTS

We thank D. Göckeritz-Dujmovic for the preparation of the organotypic slice cultures preparation, S. Giger and H. Kasper for technical support, and F. David and P. Morciano for IT support. We thank John Lisman for contributing to experimental design, and Beat Gähwiler for discussions of the results.

AUTHOR CONTRIBUTION

F.B. designed with U.G. the experiments. F.B. performed electrophysiological and calcium imaging experiments and analyzed data. S.C. performed calcium imaging experiments and analyzed data. R.L. analyzed data. F. H. designed experiments. F.B and A.H., U.G. wrote the paper.

REFERENCES

Amaral DG, Witter MP (1989) The three-dimensional organization of the hippocampal formation: a review of anatomical data. Neuroscience 31(3):571–591.

Antic SD, Zhou W-L, Moore AR, Short SM, Ikonomu KD (2010) The decade of the dendritic NMDA spike. J Neurosci Res 88 (14):2991–3001.

Ariav G, Polsky A, Schiller J (2003) Submillisecond precision of the input-output transformation function mediated by fast sodium dendritic spikes in basal dendrites of CA1 pyramidal neurons. J Neurosci 23(21):7750–7758.

Augustinaite S, Kuhn B, Helm PJ, Heggelund P (2014) NMDA spike/plateau potentials in dendrites of thalamocortical neurons. J Neurosci 34(33):10892–10905.

Basu J, Zaremba JD, Cheung SK, Hitti FL, Zemelman BV, Losonczy A, Siegelbaum SA (2016) Gating of hippocampal activity, plasticity, and memory by entorhinal cortex long-range inhibition. Science 351(6269).

Bono J, Clopath C (2017) Modeling somatic and dendritic spike mediated plasticity at the single neuron and network level. Nat Commun 8(1):1–17.

Branco T, Häusser M (2010) The single dendritic branch as a fundamental functional unit in the nervous system. Curr Opin Neurobiol 20(4):494–502.

Branco T, Clark BA, Hausser M (2010) Dendritic discrimination of temporal input sequences in cortical neurons. Science 329 (5999):1671–1675.

Branco T, Häusser M (2011) Synaptic integration gradients in single cortical pyramidal cell dendrites. Neuron 69(5):885–892.

Brandalise F, Gerber U (2014) Mossy fiber-evoked subthreshold responses induce timing-dependent plasticity at hippocampal CA3 recurrent synapses. Proc Natl Acad Sci U S A 111 (11):4303–4308.

Brandalise F, Carta S, Helmchen F, Lisman J, Gerber U (2016) Dendritic NMDA spikes are necessary for timing-dependent associative LTP in CA3 pyramidal cells. Nat Commun 7(1):1–9.

Cash S, Yuste R (1998) Input summation by cultured pyramidal neurons is linear and position-independent. J Neurosci 18 (1):10–15.

Cash S, Yuste R (1999) Linear summation of excitatory inputs by CA1 pyramidal neurons. Neuron 22(2):383–394.

Chalifoux JR, Carter AG (2011) Glutamate spillover promotes the generation of NMDA spikes. J Neurosci 31(45):16435–16446.

Cichon J, Gan W-B (2015) Branch-specific dendritic Ca2+ spikes cause persistent synaptic plasticity. Nature 520(7546):180–185.

Debanne D, Guerineau NC, Gahwiler BH, Thompson SM (1995) Physiology and pharmacology of unitary synaptic connections between pairs of cells in areas CA3 and CA1 of rat hippocampal slice cultures. J Neurophysiol 73(3):1282–1294.

Doron M, Chindemi G, Muller E, Markram H, Segev I (2017) Timed synaptic inhibition shapes NMDA spikes, influencing local dendritic processing and global I/O properties of cortical neurons. Cell Rep 21(6):1550–1561.

Dorsett C, Philpot BD, Smith SL, Smith IT (2021) The impact of SST and PV interneurons on nonlinear synaptic integration in the neocortex. Eneuro 8(5).

Dudman JT, Tsay D, Siegelbaum SA (2007) A role for synaptic inputs at distal dendrites: instructive signals for hippocampal long-term plasticity. Neuron 56(5):866–879.

Gambino F, Pagès S, Kehayas V, Baptista D, Tatti R, Carleton A, Holtmaat A (2014) Sensory-evoked LTP driven by dendritic plateau potentials in vivo. Nature 515(7525):116–119.

Gähwiler BH (1981) Organotypic monolayer cultures of nervous tissue. J Neurosci Methods 4(4):329–342.

Gidon A, Segev I (2012) Principles governing the operation of synaptic inhibition in dendrites. Neuron 75(2):330–341.

Golding NL, Spruston N (1998) Dendritic sodium spikes are variable triggers of axonal action potentials in hippocampal CA1 pyramidal neurons. Neuron 21(5):1189–1200.

Golding NL, Staff NP, Spruston N (2002) Dendritic spikes as a mechanism for cooperative long-term potentiation. Nature 418 (6895):326–331.

Grienberger C, Chen X, Konnerth A (2014) NMDA receptor-dependent multidendrite Ca2+ spikes required for hippocampal burst firing in vivo. Neuron 81(6):1274–1281.

Hardie J, Spruston N (2009) Synaptic depolarization is more effective than back-propagating action potentials during induction of associative long-term potentiation in hippocampal pyramidal neurons. J Neurosci 29(10):3233–3241.

Hawkins J, Ahmad S (2016) Why neurons have thousands of synapses, a theory of sequence memory in neocortex. Front Neural Circuits 10:23.

Henze DA, Wittner L, Buzsáki G (2002) Single granule cells reliably discharge targets in the hippocampal CA3 network in vivo. Nat Neurosci 5(8):790–795.

Humphries R, Mellor J, O'Donnell C (2021) Acetylcholine boosts dendritic NMDA spikes in a CA3 pyramidal neuron model. *bioRxiv*.

Kamiya H, Shinozaki H, Yamamoto C (1996) Activation of metabotropic glutamate receptor type 2/3 suppresses transmission at rat hippocampal mossy fibre synapses. J Physiol 493(2):447–455.

Kampa BM, Letzkus JJ, Stuart GJ (2006) Requirement of dendritic calcium spikes for induction of spike-timing-dependent synaptic plasticity. J Physiol 574(1):283–290.

Kastellakis G, Cai DJ, Mednick SC, Silva AJ, Poirazi P (2015) Synaptic clustering within dendrites: an emerging theory of memory formation. Prog Neurobiol 126:19–35.

Kastellakis G, Poirazi P (2019) Synaptic clustering and memory formation. Front Mol Neurosci 12:300.

Kim Y, Hsu CL, Cembrowski MS, Mensh BD, Spruston N (2015) Dendritic sodium spikes are required for long-term potentiation at distal synapses on hippocampal pyramidal neurons. Elife 4 e06414.

Kleindienst T, Winnubst J, Roth-Alpermann C, Bonhoeffer T, Lohmann C (2011) Activity-dependent clustering of functional synaptic inputs on developing hippocampal dendrites. Neuron 72 (6):1012–1024.

Kumar A, Schiff O, Barkai E, Mel BW, Poleg-Polsky A, Schiller J (2018) NMDA spikes mediate amplification of inputs in the rat piriform cortex. *Elife*, 7, e38446.

Langer D, van't Hoff M, Keller AJ, Nagaraja C, Pfäffli OA, Göldi M, Kasper H, Helmchen F (2013) HelioScan: a software framework for controlling in vivo microscopy setups with high hardware flexibility, functional diversity and extendibility. J Neurosci Methods 215(1):38–52.

Larkum ME, Nevian T (2008) Synaptic clustering by dendritic signalling mechanisms. Curr Opin Neurobiol 18(3):321–331.

Lisman J (2017) Glutamatergic synapses are structurally and biochemically complex because of multiple plasticity processes: long-term potentiation, long-term depression, short-term potentiation and scaling. Philos Trans R Society B: Biol Sci 372 (1715):20160260.

Lisman J, Spruston N (2005) Postsynaptic depolarization requirements for LTP and LTD: a critique of spike timing-dependent plasticity. Nat Neurosci 8(7):839–841.

Lisman J, Spruston N (2010) Questions about STDP as a general model of synaptic plasticity. Front Synaptic Neurosci 2:140.

London M, Häusser M (2005) Dendritic computation. Annu Rev Neurosci 28(1):503–532.

Losonczy A, Makara JK, Magee JC (2008) Compartmentalized dendritic plasticity and input feature storage in neurons. Nature 452(7186):436–441.

Lovett-Barron M, Turi GF, Kaifosh P, Lee PH, Bolze F, Sun X-H, Nicoud J-F, Zemelman BV, Sternson SM, Losonczy A (2012) Regulation of neuronal input transformations by tunable dendritic inhibition. Nat Neurosci 15(3):423–430.

Major G, Larkum ME, Schiller J (2013) Active properties of neocortical pyramidal neuron dendrites. Annu Rev Neurosci 36 (1):1–24.

Major G, Polsky A, Denk W, Schiller J, Tank DW (2008) Spatiotemporally graded NMDA spike/plateau potentials in basal dendrites of neocortical pyramidal neurons. J Neurophysiol 99 (5):2584–2601.

Makara J, Magee J (2013) Variable dendritic integration in hippocampal CA3 pyramidal neurons. Neuron 80(6):1438–1450.

Mel BW, Schiller J, Poirazi P (2017) Synaptic plasticity in dendrites: complications and coping strategies. Curr Opin Neurobiol 43:177–186.

Mori M, Abegg MH, Gähwiler BH, Gerber U (2004) A frequency-dependent switch from inhibition to excitation in a hippocampal unitary circuit. Nature 431(7007):453–456.

Müllner F, Wierenga C, Bonhoeffer T (2015) Precision of inhibition: dendritic inhibition by individual GABAergic synapses on hippocampal pyramidal cells is confined in space and time. Neuron 87(3):576–589.

Murayama M, Pérez-Garci E, Nevian T, Bock T, Senn W, Larkum ME (2009) Dendritic encoding of sensory stimuli controlled by deep cortical interneurons. Nature 457(7233):1137–1141.

Oikonomou KD, Short SM, Rich MT, Antic SD (2012) Extrasynaptic glutamate receptor activation as cellular bases for dynamic range compression in pyramidal neurons. Front Physiol 3:334.

Poirazi P, Papoutsi A (2020) Illuminating dendritic function with computational models. Nat Rev Neurosci 21(6):303–321.

Polsky A, Mel BW, Schiller J (2004) Computational subunits in thin dendrites of pyramidal cells. Nat Neurosci 7(6):621–627.

Rancz EA, Häusser M (2006) Dendritic calcium spikes are tunable triggers of cannabinoid release and short-term synaptic plasticity in cerebellar Purkinje neurons. J Neurosci 26(20):5428–5437.

Rashid SK, Pedrosa V, Dufour MA, Moore JJ, Chavlis S, Delatorre RG, Basu J (2020) The dendritic spatial code: branch-specific place tuning and its experience-dependent decoupling. *bioRxiv*.

Remy S, Spruston N (2007) Dendritic spikes induce single-burst long-term potentiation. Proc Natl Acad Sci U S A 104 (43):17192–17197.

Please cite this article in press as: Brandalise F et al. Dendritic Branch-constrained N-Methyl-D-Aspartate Receptor-mediated Spikes Drive Synaptic Plasticity in Hippocampal CA3 Pyramidal Cells. Neuroscience (2021), https://doi.org/10.1016/j.neuroscience.2021.10.002

Remy S, Csicsvari J, Beck H (2009) Activity-dependent control of neuronal output by local and global dendritic spike attenuation. Neuron 61(6):906–916.

Salin PA, Scanziani M, Malenka RC, Nicoll RA (1996) Distinct short-term plasticity at two excitatory synapses in the hippocampus. Proc Natl Acad Sci U S A 93(23):13304–13309.

Schiller J, Major G, Koester HJ, Schiller Y (2000) NMDA spikes in basal dendrites of cortical pyramidal neurons. Nature 404 (6775):285–289.

Sheffield ME, Dombeck DA (2015) Calcium transient prevalence across the dendritic arbour predicts place field properties. Nature 517(7533):200–204.

Sheffield MEJ, Adoff MD, Dombeck DA (2017) Increased prevalence of calcium transients across the dendritic arbor during place field formation. Neuron 96(2):490–504.e5.

Soldado-Magraner S, Brandalise F, Honnuraiah S, Pfeiffer M, Moulinier M, Gerber U, Douglas R (2020) Conditioning by subthreshold synaptic input changes the intrinsic firing pattern of CA3 hippocampal neurons. J Neurophysiol 123(1):90–106.

Spruston N (2008) Pyramidal neurons: dendritic structure and synaptic integration. Nat Rev Neurosci 9(3):206–221.

Stuart GJ, Spruston N (2015) Dendritic integration: 60 years of progress. Nat Neurosci 18(12):1713–1721.

Suzuki M, Larkum ME (2017) Dendritic calcium spikes are clearly detectable at the cortical surface. Nat Commun 8(1):1–11.

Topolnik L, Camiré O (2019) Non-linear calcium signalling and synaptic plasticity in interneurons. Curr Opin Neurobiol 54:98–103.

Williams LE, Holtmaat A (2019) Higher-order thalamocortical inputs gate synaptic long-term potentiation via disinhibition. Neuron 101 (1):91–102.e4.

(Received 18 March 2021, Accepted 3 October 2021)
(Available online xxxx)